

Experimental comparison of piezoelectric and magnetostrictive shunt dampers

Vivake M. Asnani^{*a}, Zhangxian Deng^b, Justin J. Scheidler^c, Marcelo J. Dapino^b

^aMaterials and Structures Division, NASA Glenn Research Center, Cleveland, OH, 44135; ^bNSF I/UCRC on Smart Vehicle Concepts, Department of Mechanical & Aerospace Engineering, The Ohio State University, Columbus, OH 43210; ^cUniversities Space Research Association, NASA Glenn Research Center, Cleveland, OH 44135

ABSTRACT

A novel mechanism called the vibration ring is being developed to enable energy conversion elements to be incorporated into the driveline of a helicopter or other rotating machines. Unwanted vibration is transduced into electrical energy, which provides a damping effect on the driveline. The generated electrical energy may also be used to power other devices (e.g., health monitoring sensors). PZT ('piezoceramic') and PMN-30%PT ('single crystal') stacks, as well as a $Tb_{0.3}Dy_{0.7}Fe_{1.92}$ ('Terfenol-D') rod with a bias magnet array and a pickup coil, were tested as alternative energy conversion elements to use within the vibration ring. They were tuned for broadband damping using shunt resistors, and dynamic compression testing was conducted in a high-speed load frame. Energy conversion was experimentally optimized at 750Hz by tuning the applied bias stress and resistance values. Dynamic testing was conducted up to 1000Hz to determine the effective compressive modulus, shunt loss factor, internal loss factor, and total loss factor. Some of the trends of modulus and internal loss factor versus frequency were unexplained. The single crystal device exhibited the greatest shunt loss factor whereas the Terfenol-D device had the highest internal and total loss factors. Simulations revealed that internal losses in the Terfenol-D device were elevated by eddy current effects, and an improved magnetic circuit could enhance its shunt damping capabilities. Alternatively, the Terfenol-D device may be simplified to utilize only the eddy current dissipation mechanism (no pickup coil or shunt) to create broadband damping.

Keywords: Shunt damping, driveline vibration, piezoelectric, magnetostrictive

1. INTRODUCTION

In machines power is often transferred through rotating mechanical systems, which has the side effect of generating vibration. This can create functional issues like loss of precision in a cutting tool. It can also generate unwanted noise, such as gearbox-induced noise within a helicopter cabin. Once vibration energy spreads throughout a machine it becomes very difficult to control; thus it is ideal to attenuate vibration as close to the source as possible. The vibration ring, depicted in Fig 1., is a novel mechanism that is being developed to incorporate vibration damping elements into a machine's driveline.¹ The device may be installed in-between any two components, such as between a gear and shaft or a bearing and its housing. It uses a series of mechanical links to direct driveline vibration through the damping elements in order to remove vibratory energy from the system.

Shunted piezoelectric ceramic stacks and magnetostrictive metal rods are being considered for use within the vibration ring. These elements can provide damping and have high enough stiffness to be incorporated within a rotating system assembly. The stacks are constructed from layers of poled piezoelectric material, and can transduce energy between the mechanical and electrical domains. Magnetostrictive metal rods can transduce energy between mechanical and magnetic domains and are wrapped in a coil of wire to couple with the electrical domain. Either of these elements may be configured as a vibration damping device by connecting its electrical terminals to a resistive shunt circuit^{2,3}. In this arrangement, the electrical energy that is generated is removed from the system to create a net damping effect. The shunt may be a passive circuit including electrical resistors to convert the vibration energy to heat or a harvesting circuit that stores the energy to power other devices (e.g., health monitoring sensors). The shunt circuit may also be adaptively tuned to vary the frequency response of stiffness and damping.⁴

*vivake.m.asnani@nasa.gov

Along with the energy loss via the shunt circuit, there are a series of energy loss mechanisms internal to these devices. For example, dielectric losses in piezoelectric ceramics have been shown to be significant⁵, while magnetostrictive rods exhibit significant magnetic energy dissipation in the form of hysteresis⁶ and frequency-dependent eddy current losses⁷. In addition, current generated in the pickup coil will produce Joule heat. These loss mechanisms add to the total damping, but they reduce the electrical energy generated. Thus, internal losses reduce the capability of the shunt circuit to tune the mechanical response or harvest energy.

As a part of the development process for the vibration ring, the frequency response characteristics of candidate shunt damping elements needed to be compared. Shunt damping models are available for this purpose,^{2,8} but they require estimates of the device properties (e.g., energy coupling factors). Parameterization may be accomplished using an actuation-based resonance technique,⁹ but the resulting properties are frequency independent and do not comprehensively represent the loss effects. As a result of these limitations, two separate dynamic load frame experiments were conducted to characterize several shunted piezoelectric stacks and a Terfenol-D rod-based shunt damping device.^{10,11} Select results from two of the more common stack types (PZT and PMN-PT) and the Terfenol-D device are examined here with a focus on comparing the frequency dependence of stiffness, internal damping, and shunt damping.

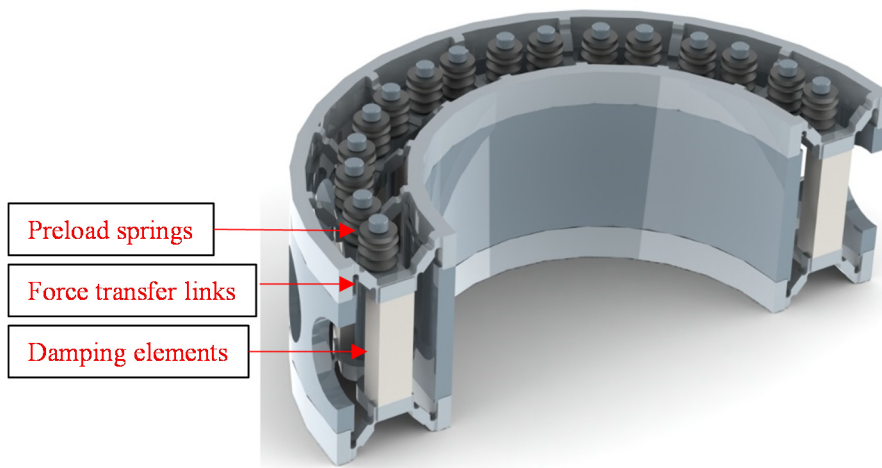


Figure 1. The vibration ring mechanism.

2. DESCRIPTION OF EXPERIMENT

2.1 Test articles and experimental system

The piezoelectric stacks tested are illustrated in Fig. 2 and described in Table 1. Both stacks are approximately 16mm tall and were constructed by gluing together 5mm x 5mm square piezoelectric plates. Inactive ceramic plates were used on the top and bottom for electrical isolation. The piezoelectric plates have electrodes on their faces, which are electrically connected in parallel to a single set of wires. The ‘piezoceramic’ device is a commercial device made from co-fired polycrystalline PZT plates, while the ‘single crystal’ device is a custom device made with monolithic PMN-30%PT plates. The Terfenol-D device, illustrated in Fig. 3 and described in Table 1, includes a 7mm diameter, 10mm long $Tb_{0.3}Dy_{0.7}Fe_{1.92}$ rod, which was wrapped in a pickup coil and biased using a magnetic circuit. The number of turns and wire gauge of the pickup coil were optimized using a COMSOL simulation-based method with the objective to maximize its electrical energy output.³ The magnetic circuit was designed to shift the region of maximum magnetic response sensitivity (the so called burst region) into the range of the applied loads of the experiment.¹¹ The source of magnetic flux is an array of permanent magnets positioned around the rod and coil using an aluminum fixture. The flux is guided through the rod using the steel load testing platens that contact its top and bottom faces. Each of the three devices were ground flat and parallel to allow for even face contact during compression testing.

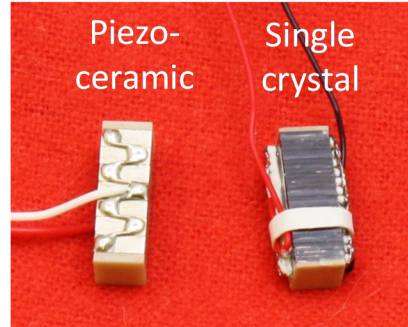


Figure 2. Piezoelectric stacks used as damping devices.

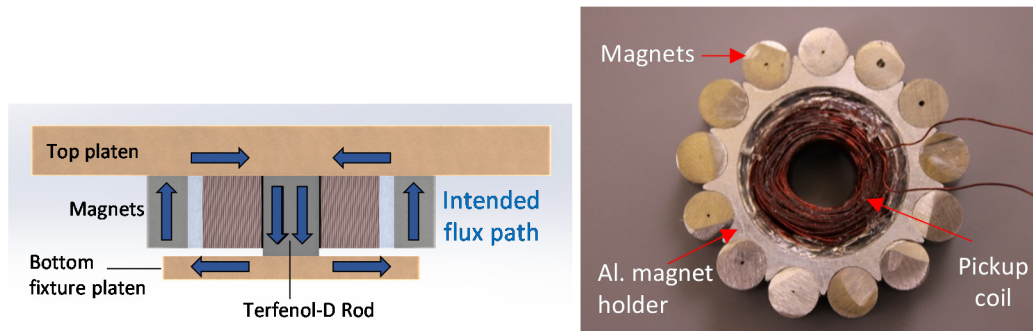


Figure 3. Terfenol-D damping device - schematic of magnetic circuit (left) and picture of circuit components (right).

Table 1. Damping device information.

Device name	Material	Assembly
Piezoceramic	Noliac NCE51F, soft-doped polycrystalline PZT , 5mm x 5mm square, 0.05mm thick.	Noliac model NAC2013-H16-A0, 7 active plates, 33 co-fired layers/plate, 2 inactive ceramic end plates, total height 15.89mm.
Single crystal	TRS Technologies X2B, single crystal PMN-30%PT , 5mm x 5mm square, 0.5mm thick.	Custom assembly by Micromechanics Inc., 28 active plates, 2 inactive ceramic end plates, total height 15.99mm.
Terfenol-D	Etrema Products, Inc. Tb_{0.3}Dy_{0.7}Fe_{1.92} rod, 7mm diameter, 10mm long.	Custom assembly by authors. Rod is encased by a 500-turn 30AWG pickup coil, and an array of Alnico grade 8 bias magnets. ¹¹

A dynamic load frame (MTS 831.50 Elastomer Test System) was used to apply bias and sinusoidal compressive forces to the devices up to 1000Hz. The test setups for the piezoelectric and magnetostrictive devices are illustrated in Fig. 4. In both setups the load train was driven by a servo-hydraulically controlled piston and the devices were compressed using a metal platen. Beneath the devices were metal fixtures that also held capacitive displacement probes on the left and right sides of the devices. The probes observe the motions of the top platen relative to the bottom fixture, and their signals were averaged to provide a measure of the device displacement. Beneath the fixture was a load cell to observe the force experienced by the device.

Several design precautions were taken to reduce potential sources of experimental error. The fixtures and platens were designed using finite element analysis, such that they did not have significant dynamic deformations that would corrupt the probe measurements. At the same time, the fixture masses and other mass beneath the device were minimized such

that inertial force error in the load cell measurement was limited to 0.5% at 1000Hz.^{10,11} For the Terfenol-D setup this required that the magnet array be mounted to the upper platen instead of resting on the bottom fixture. The coil with nested rod were also moved to the upper platen to prevent the magnet array from moving respect to the coil and generating electrical noise. The attraction between the magnet array and bottom fixture did create a DC offset in the load cell measurement, but this was removed in calibration. Change in this attractive force, due to the position change of the magnet array during compression testing, was verified to be negligibly small. Flush contact with the device was established by incorporating a spherical seat and the contact conditions were verified prior to each test setup using a pressure film sensor (Fuji Prescale).^{10,11} The moving mass above the device was also minimized to drive any potential resonances up in frequency.

The magnitude of each sensor channel was calibrated at DC and then verified up to 1000 Hz. The phase was then calibrated over the range from 2Hz to 1000 Hz to account for time delay differences between measurement channels.¹⁰ This step was critical to accuracy quantify loss metrics, which depend on relative the phase between signals. Preliminary testing revealed a system resonance, which fell into the range from 1000 Hz to 1200 Hz, depending on the device that was installed. The resonance affected the system by causing the upper platen to dynamically tilt. In all cases testing was done up to 1000Hz, but the data reported here is limited to that which was not affected by the resonance. For the piezoceramic and single-crystal devices, the data reported is limited to 923 Hz and 804 Hz, respectively. The Terfenol-D device responded somewhat non-linearly to applied load, and its 2nd and 3rd harmonic frequency components activated the system resonance. As a result the reported data is limited to 350Hz.

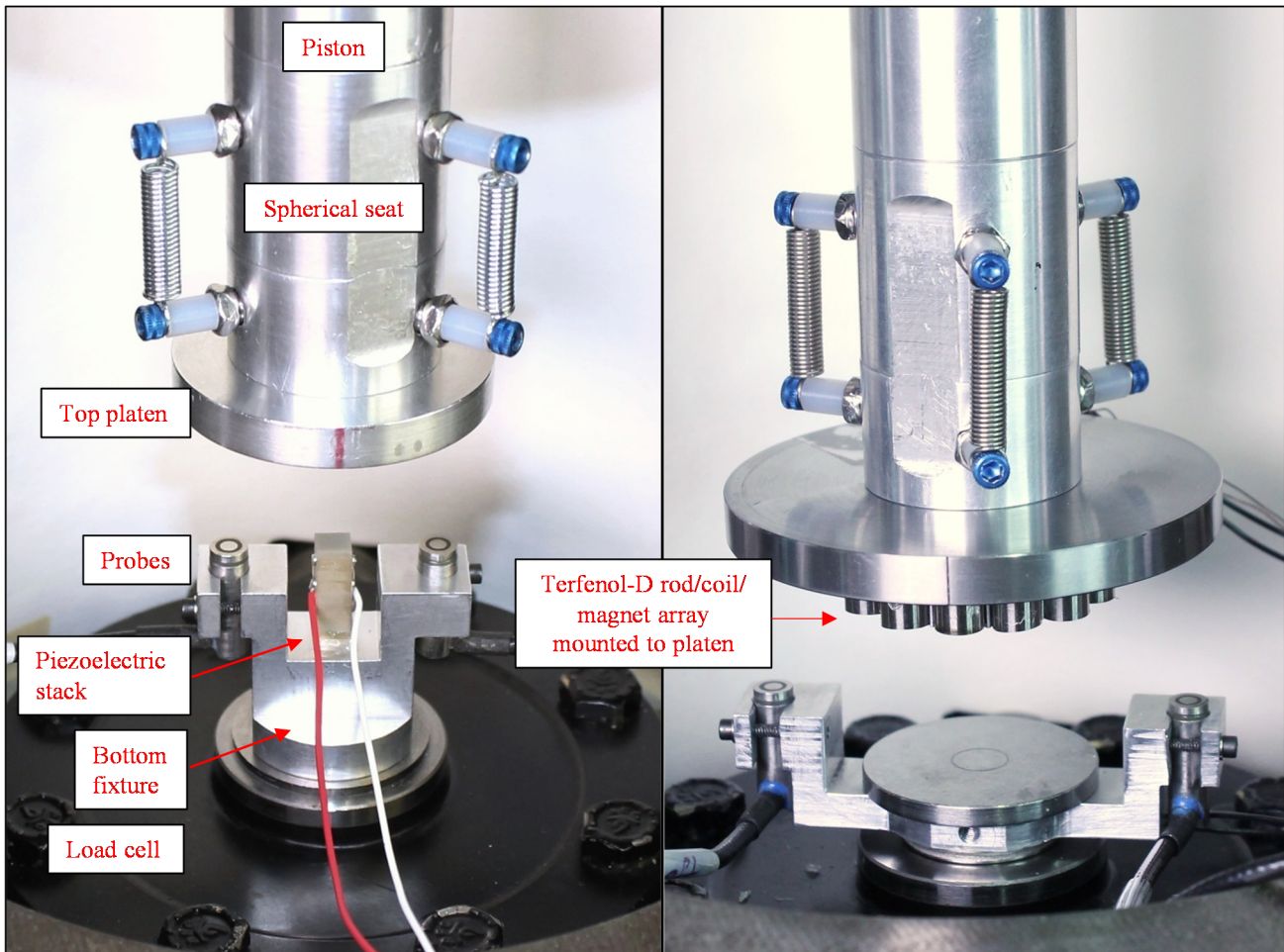


Figure 4. Load frame test setups for piezoelectric (left) and Terfenol-D (right) device testing.

2.2 Test method and data processing

Sensor data was acquired through 10 kHz anti-aliasing filters at a sampling rate of 40 kHz. In all tests the system's response to the applied force was allowed to reach steady-state before the sensor data was saved. One second of data was captured and transformed into the frequency domain (discrete Fourier transform), which provided a frequency resolution of 1 Hz. The left and right probe displacements were then averaged to produce an estimate of the device displacement. Subsequently, the 1st harmonic components (i.e., complex valued phasors) of force F displacement X and shunt voltage V were extracted for further processing. Calculations of stiffness and loss factor were done in a manner that is consistent with the standard for load frame characterization of elastomeric materials,¹² such that the results here may be compared with typical vibration reduction components. The complex stiffness of the device was computed as,

$$\tilde{k} = \frac{F}{X}. \quad (1)$$

When internal mass effects are small, complex stiffness may be expanded into the form $\tilde{k} = k(1 + j\eta)$, where k is the (lossless) stiffness and η is the loss factor.¹³ Accordingly these component were computed as,

$$k = \text{Re}\{\tilde{k}\} \quad (2)$$

and

$$\eta = \frac{\text{Im}\{\tilde{k}\}}{k}. \quad (3)$$

In order to compare devices of different geometry, the stiffness was normalized to create an effective compressive modulus using the equation,

$$E = \frac{k \cdot h}{A}, \quad (4)$$

where h is the total height and A is the cross sectional area of the piezoelectric stack or Terfenol-D rod. The complex stiffness expansion was originally derived based on the definition of the loss factor metric, $\eta := (W_{\text{loss}}/2\pi)/W_{\text{osc}}$. I.e. the loss factor is proportional to the energy dissipated by the complex spring per cycle W_{loss} normalized by the oscillation energy that gets returned to the source per cycle W_{osc} when the spring is operating in steady-state. Thus, the loss factor metric may be broken into parts associated with the energy components that contribute to the total dissipation. First, the energy dissipated in the shunt per cycle is computed as,

$$W_{\text{shunt}} = \frac{T_o |V|^2}{2R_L}, \quad (5)$$

where T_o is the period of oscillation and R_L is the shunt resistance. Then the oscillation energy is calculated as follows, based on the energy storage at maximum compression,

$$W_{\text{osc}} = \frac{1}{2}k|X|^2. \quad (6)$$

The *shunt loss factor*, or the component of the loss factor associated with energy dissipation in the shunt, was then computed as,

$$\eta_{\text{shunt}} = \frac{W_{\text{shunt}}/2\pi}{W_{\text{osc}}}. \quad (7)$$

Then the *internal loss factor*, or the component of the loss factor associated with the device, was computed as,

$$\eta_{\text{int}} = \eta - \eta_{\text{shunt}}. \quad (8)$$

For the piezoelectric devices, the internal loss factor includes all losses that occur within the stack. For the Terfenol-D device, this metric represents the loss in the rod, as well as those within the magnetic circuit and pickup coil.

Metrics were also used to optimize the prestress applied to the devices, with the goal of achieving the highest coupling between mechanical and electrical domains. For the piezoelectric devices, the optimization was based on the following estimate of the electromechanical coupling factor,¹

$$\kappa' = \sqrt{1 - k_{sc}/k_{oc}}. \quad (9)$$

Here k_{sc} and k_{oc} are the stiffness values measured at the targeted center frequency for damping, 750 Hz, under short and open circuit conditions, respectively. This estimate was derived assuming zero energy loss within the device, but it is assumed to follow the same trend as the true value when evaluate against prestress. For the Terfenol-D device, the optimum prestress was considered to be that which maximized the voltage magnitude, $|V|$, resulting from quasi-statically applied force under open-circuit conditions. This relationship is not as well defined and requires more assumptions. The open-circuit voltage magnitude has been shown to be proportional to the piezomagnetic constant,¹¹ and the piezomagnetic constant has been shown experimentally to be maximized by the same prestress as the magnetomechanical coupling factor,¹⁴ and finally the magnetomechanical coupling factor is assumed to be directly related to the electromechanical coupling. This method also assumes that the optimal quasi-static prestress is equivalent to the optimal dynamic prestress.

Testing was implemented in three stages using the nominal conditions listed in Table 2. In the first stage the prestress \bar{T} was optimized. For all devices the prestress was varied in steps while dynamic stress was applied. For the piezoelectric devices, data was collected in open and short circuit conditions and then the electromechanical coupling factor was estimated using equation above. At first, the dynamic stress was set to a small value T_{small} to create a high resolution mapping between coupling factor and prestress. The approximate optimal prestress was found and then the dynamic stress was increased to its nominal value T and the coupling factor was re-measured over the local region. The value of prestress that created the largest electromechanical coupling factor under nominal conditions was selected. For the Terfenol-D device, the nominal value of dynamic stress was used and the prestress that maximized the voltage magnitude was selected.

In the second stage of testing, the shunt resistance was optimized. Using the optimal prestress the nominal dynamic stress was applied at 750 Hz, and the shunt resistance was varied with a resolution of 1Ω . For the piezoelectric devices, the shunt resistance that produced the highest loss factor was selected as the optimum value. For the Terfenol-D device, the loss factor increased monotonically toward an open circuit, indicating that the internal loss trend was masking the effect of the shunt loss. After this finding, the criteria was changed and the Terfenol-D shunt resistance was optimized based on the shunt loss factor. In the third stage, the frequency response was found. The optimal prestress and optimal shunt resistance were applied, and then the nominal dynamic stress was applied in frequency steps from 2Hz to 1000Hz. For each step the effective compressive modulus, shunt loss factor, internal loss factor, and total loss factor were computed.

Table 2. Nominal test conditions.

	1. Optimizing prestress	2. Optimizing resistance	3. Measuring frequency response
Piezoceramic and single crystal:	$R_L = \{0, \infty\}$ $\bar{T} \in [3.0, 32] \text{MPa}$ $f = 750 \text{Hz}$ $T_{small} = 2.0 \text{MPa}$	R_L : Varied \bar{T} : Optimal $f = 750 \text{Hz}$	R_L, \bar{T} : Optimal $f = [2, 1000] \text{Hz}$
Terfenol-D:	$R_L = \infty$ $\bar{T} \in [8.3, 14.2] \text{MPa}$ $f = 5 \text{Hz}$		
All:	T : $\underbrace{8.0 \text{MPa}}_{\text{Piezoceramic}}, \underbrace{4.0 \text{MPa}}_{\text{Single crystal}}, \underbrace{7.3 \text{MPa}}_{\text{Terfenol-D}}$		

3. RESULTS AND DISCUSSION

Results from the prestress optimization are shown in Fig. 5. The left plot shows the coupling factor estimate vs. prestress for the piezoelectric devices computed using the small value of dynamic stress. Both devices initially increase in coupling with applied prestress. At about 8 MPa the piezoceramic curve flattens out. On the other hand there is a distinct peak around 8 MPa for the single crystal device. Using the nominal dynamic stress, the optimal values of prestress were found to be 20 MPa for the piezoceramic device and 10 MPa for the single crystal device. The right plot in Fig. 5 shows the results from optimizing the prestress of the Terfenol-D device. The voltage magnitude increased as the prestress was reduced toward zero, indicating that the optimum prestress would be in the tensile region. In order to shift the optimum prestress into the compressive region a stronger bias magnetic field would be required. For this experiment, the prestress was selected to be 8.3 MPa, which was the smallest compressive prestress that could be applied without losing contact with the device during dynamic testing.

The optimal shunt resistance values found were to be 129.3 Ω , 1801 Ω , and 31.7 Ω , respectively, for the piezoceramic, single crystal, and Terfenol-D devices.

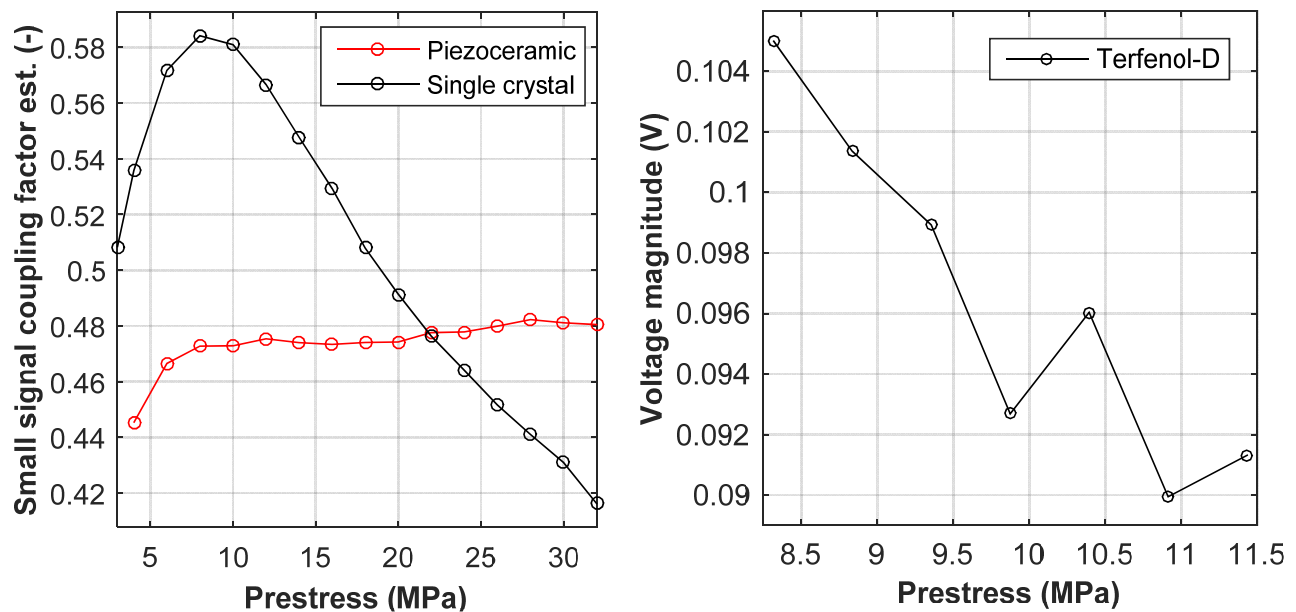


Figure 5. Prestress optimization curves for the piezoelectric (left) and Terfenol-D (right) devices.

Frequency response curves generated from testing the optimized shunt dampers are shown in Fig. 6. The quasi-static moduli of the single crystal and Terfenol-D devices were similar, 13.3 GPa and 16.0 GPa, respectively. However, the piezoceramic was about twice as stiff, having a quasi-static modulus of 29.1 GPa. Both piezoelectric devices increased their moduli monotonically with frequency and exhibited a sharp upturn after 300 Hz. Increases in moduli are expected, because frequency increases should lead to greater charge generation and in-turn greater field opposing electric domain rotation. One would expect a similar trend from the Terfenol-D device, as increased frequency should generate larger currents in the coil, and in-response generate a field that opposes magnetic domain rotation. However, the device initially gets softer with frequency, and then begins to increase after 100Hz. The initial softening is unexplained at this point.

The shunt loss factor curves are generally bell shaped, starting at zero for the quasi-static condition and reaching a peak at or near 750 Hz. The peak shunt loss factor of the single crystal is greatest at 0.182, followed by the piezoceramic at 0.129. At the maximum data point of 350Hz, the Terfenol-D shunt loss factor is 0.041.

At the quasi-static condition the internal losses were 0.055, 0.074, and 0.105, respectively, for the piezoceramic, single crystal, and Terfenol-D dampers. For the two piezoelectric devices, the internal losses start to decrease noticeable after about 300 Hz, at the same time as the upturn in moduli. For the Terfenol-D device, however, the internal loss appears to

be more directly related to its modulus trend. The loss decreases at first, and then after about 30Hz begins to increase sharply. The sharp, almost linear, increase with frequency is consistent with eddy current type losses. However, this experiment was conducted well below the frequency where eddy current losses within the rod should be significant (below the magnetic diffusion cutoff frequency).⁷ To investigate this, the magnetic circuit used in this experiment was simulated using a 3D model in COMSOL. The results revealed that part of the generated magnetic energy was being dissipated through eddy currents in the aluminum magnet holder. Thus, it is likely that a prototype that used a non-electrically-conductive material to hold the magnets should have significantly lower internal loss and significantly greater shunt loss. This finding also implies that a simplified damper could be designed without a coil or shunt, using only the eddy current effect to create broadband damping.

At 750 Hz the piezoceramic and single crystal devices had total loss factors of 0.171 and 0.252, respectively. At 350 Hz the Terfenol-D device reached a total loss factor of 0.247 and appeared to still be increasing. At 350 Hz and below, where data was available for all cases, the Terfenol-D device had the greatest total loss factor.

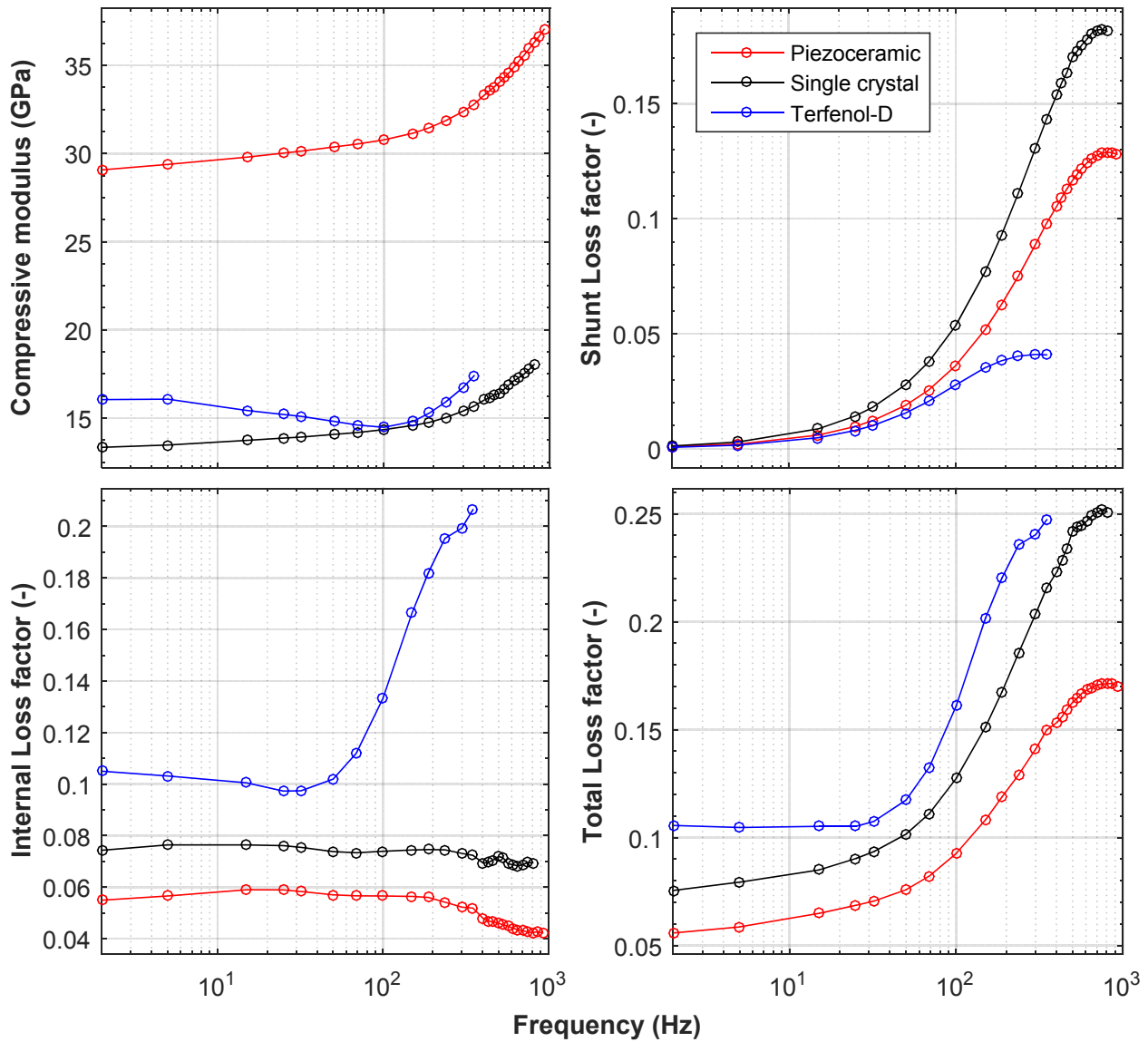


Figure 6. Frequency responses of the optimized shunt dampers tuned to 750Hz.

4. CONCLUSION

Dynamic response characteristics of three high-stiffness, broadband shunt damping devices, constructed from PZT ('piezoceramic'), PMN-30%PT ('single crystal'), and $\text{Tb}_{0.3}\text{Dy}_{0.7}\text{Fe}_{1.92}$ ('Terfenol-D'), were evaluated up to 1000 Hz using a series of carefully-controlled load frame experiments. Compressive bias and dynamic forces were applied while energy was dissipated from the devices using a shunt resistance. Phase aligned force, displacement, and voltage signals were used to compute the effective compressive modulus, internal loss factor, shunt loss factor, and total loss factor metrics versus frequency. The shunt loss factor was computed based on the energy dissipated by the shunt, and as such represented the capability for energy harvesting and the component of the total loss factor that could be tuned using the shunt. The internal loss factor was the component of the total loss factor based on energy dissipated within the device. For each device, the optimal prestress was found to maximize the mechanical-to-electrical energy conversion. Then, the resistance was optimized to maximize the shunt loss factor at 750 Hz. Finally, the optimized devices were tested in the range from 2 Hz to 1000 Hz. The data reported here was limited to 923 Hz, 804 Hz, and 350 Hz, respectively, for the piezoceramic, single crystal, and Terfenol-D damping devices, due to the influence of a resonance in the loading system.

The energy coupling of the single crystal device was found to be much more sensitive to prestress than the piezoceramic, and they had optimal prestress values of 10 MPa and 20 MPa, respectively. The optimal prestress for the Terfenol-D device was found to be in the tensile region, and so the compressive prestress applied was set to be as small as possible while maintaining contact.

For the piezoceramic device, the quasi-static modulus (29.1 GPa) was about twice that of the single crystal and Terfenol-D devices (13.3 GPa and 16.0 GPa, respectively). As expected, both piezoelectric devices exhibited electric field-induced stiffening with increased frequency. However, the modulus of the Terfenol-D device was initially reduce up to 100 Hz, after which there was a sharp upturn. The increase could be explained by magnetic field-induced stiffening, but the reason for the initial softening was not apparent.

The Terfenol-D device had the highest quasi-static internal loss factor (0.105), followed by the single crystal (0.074), and then the piezoceramic (0.055). For both piezoelectric devices, the internal loss factor appeared to be indirectly related to modulus, resulting in a slight reduction with frequency. On the other hand, the Terfenol-D device's modulus reduced slightly at first and then sharply increased after about 30 Hz. At the maximum frequency tested (350 Hz), the internal loss factor became very large (0.207). Simulations of the magnetic circuit revealed that the sharp increase in the internal loss factor was caused by eddy currents generated in the aluminum fixture used to hold the biasing magnets.

The single crystal device exhibited the greatest peak shunt loss factor at 750 Hz (0.182), followed by the piezoceramic (0.129). At the highest frequency tested (350 Hz), the shunt loss factor for the Terfenol-D device was relatively small (0.041). This is consistent with the finding that much of the magnetic energy was dissipated by eddy currents and therefore was not transduced to the electrical domain. At 750 Hz, the single crystal device had the greatest total loss factor (0.252) followed by the piezoceramic device (0.171). However, in the frequency band where the Terfenol-D damper was tested (up to 350 Hz) it had a significantly higher total loss factor than both piezoelectric devices.

The high value of shunt loss factor produced by the single crystal device indicates that it would be the preferred choice for a damper if frequency response tuning or energy harvesting were important. On the other hand, the Terfenol-D device exhibited the greatest total loss factor, despite being operated at a non-optimal magneto-mechanical bias condition. The data also suggests that the Terfenol-D shunt loss factor could be greatly improved by redesigning the biasing circuit to eliminate eddy current losses. Alternatively, it could be configured as a simplified broadband damper, with no coil or shunt, by including a high permeability, high conductivity material in the magnetic circuit.

REFERENCES

- [1] Asnani, V. M., Krantz, T. L., Delap, D. D., and Stringer, D. B., "The Vibration Ring – Seedling Fund Phase 1 Final Report," NASA/TM – 2014-218337 (2014).
- [2] Hagood, N. W. and von Flowtow, A., "Damping of structural vibrations with piezoelectric materials and passive electrical networks," *Journal of Sound and Vibration* 146(2), 243 – 268 (1991).
- [3] Deng, Z., Asnani, V. M., and Dapino, M. J., "Magnetostrictive vibration damper and energy harvester for rotating machinery," *Proc. SPIE* 9433, 94330C-1 – 94330C-11 (2015).
- [4] Fleming, A. J. and Moheimani, S. O. R., "Adaptive piezoelectric shunt damping," *Smart Materials and Structures* 12(1), 36 – 48 (2003).
- [5] Uchino, K. and Hirose, S., "Loss mechanisms in piezoelectrics: How to measure different losses separately," *IEEE Transactions on Ultrasonics, Ferroelectrics, and Frequency Control* 48(1), 307 – 321 (2001).
- [6] Bertotti, G. and Mayergoyz, I. D., [The Science of Hysteresis: Hysteresis in Materials, volume 3]. Academic Press, Oxford (2006).
- [7] Scheidler, J. J. and Dapino, M. J., "Mechanically induced magnetic diffusion in cylindrical magnetoelastic materials," *Journal of Magnetism and Magnetic Materials* 397, 233 – 239 (2016).
- [8] Fenn, R. C. and Gerber, M. J., "Passive damping and velocity sensing using magnetostrictive transduction," *Proc. SPIE* 2190, 216 – 227 (1994).
- [9] Sherrit, S., et al., "Multilayer piezoelectric stack actuator characterization," *Proc. SPIE* 6929, 692909 (2008).
- [10] Asnani, V. M. and Scheidler, J. J., "Experimental characterization of the stiffness, damping, and power generation of several shunted piezoelectric stacks for use in smart mechanical components," NASA/TM (2016).
- [11] Deng, Z., "Nonlinear modeling and characterization of the Villari effect and model-guided development of magnetostrictive energy harvesters and dampers," PhD thesis, The Ohio State University (2015).
- [12] ASTM International, "Standard guide for dynamic testing of vulcanized rubber and rubber-like materials using vibratory methods," ASTM standard D5992-96 (2011).
- [13] Ungar, E. E. and Kerwin Jr., E. M., "Loss factors of viscoelastic systems in terms of energy concepts," *Journal of the Acoustic Society of America* 34(7), 954 – 957 (1962).
- [14] Wun-Fogle, M., Restorff, J. B., and Clark, A. E., "Magnetomechanical Coupling in Stress-Annealed Fe–Ga (Galfenol) Alloys," *IEEE Transactions on Magnetics* 42(10), 3120 – 3122 (2006).